Canopy Modeling and Satellite Comparison Studies Using EO-1

James A. Smith

Background

This report gives a brief synopsis of our research studies in the comparison and use of EO-1 satellite observations with field measurements, modeling, and other satellite systems. The work is on-going. We have three study areas representing different physiographic and land cover regions where we make detailed measurements of the surface and atmospheric state, co-incident with satellite tasking. Our sites include areas near Rochester, NY, Howland, ME, and Fraser, CO. This summary principally discusses analyses from the Rochester site. Additional material is given in the references.

The Rochester site is near the shore of Lake Ontario and contains a variety of features, ranging from water of varying depths, deciduous/coniferous forest, grass fields, and urban areas. It was chosen because of its proximity to the Rochester Institute of Technology (RIT), which assisted in ground data collection. Additionally, we originally intended to compare observations with the RIT airborne multispectral scanner, especially its thermal infrared bands, with the Landsat thermal infrared band. However, our key aircraft data acquisition effort coincided with September 11, 2001, and we were not able to complete this line of attack.

But we were successful in acquiring co-incident, high resolution multispectral and thermal infrared observations from the Department of Energy Multispectral Thermal Imager (MTI) satellite. In collaboration with the Los Alamos National Laboratory, we also have obtained co-incident tasking of the MTI and EO-1 over all three of our study sites, and fieldwork and analyses continue.

The Howland, ME study site is contained within the International Paper's Northern Experimental Forest (NEF). It is a boreal--northern hardwood transitional forest consisting of hemlock-spruce-fir, aspen-birch, and hemlock-hardwood mixtures and is a MODIS validation site.

The Fraser, CO study site is contained within the U.S. Forest Service Fraser Experimental Forest. It is a high elevation site ranging from 2680 to 3900 m. Engelmann spruce and subalpine fir are the predominant trees at higher elevations or north slopes; lodgepole pine is the predominant tree at lower elevations and on drier upper slopes. The study site is part of the NASA Cold Land Processes Experiment (CLPX).

Objectives

Our initial objective was to compare the performance of the EO-1 Advanced Line Imager (ALI) with the Landsat 7 Enhanced Thematic Mapper (ETM+). Secondly, we wanted to apply calibration and atmospheric corrections to the data to compare with surface measured reflectance and predicted canopy reflectance and thermal infrared model simulations.

A long-term objective is to see if we can separate the observations of the thermal infrared versus reflectance measurements in time and from different platforms. Originally, we intended to use the ETM+ thermal infrared band. However, the DOE MTI sensor provides a better capability to test our hypotheses. Further, we found that the EO-1 Hyperion sensor provides a rich source of spectral features for comparison to our models and can be used for atmospheric corrections using its appropriate spectral bands. Our current efforts emphasize Hyperion and MTI.

Comparison of Landsat-7 ETM+ and EO-1 ALI

The ALI differs from the ETM+ in a number of ways. The pushbroom design of the ALI provides a much longer dwell time per pixel (~4 msec) than the whiskbroom ETM+ (~10 μsec), which permits 12-bit digitization of the ALI data with a single gain setting. The 10m resolution of the panchromatic band improves on the 15m resolution of the ETM+, and the ALI panchromatic band was narrowed to 0.48μm - 0.70μm from the 0.52μm - 0.90μm bandwidth on the ETM+. The ALI also has two new multispectral bands: band 1' (0.43μm - 0.45μm) and 5' (1.20μm – 1.29μm). Additionally, the ETM+ band 4 was split into bands 4 and 4' to avoid a water absorption feature. Finally, the ALI has no thermal band.

For the comparisons discussed here, we obtained ETM+ and ALI images on August 25, 2001 over the Rochester, NY area. A recent Ikonos image highlighting the area is shown below in Figure 1.

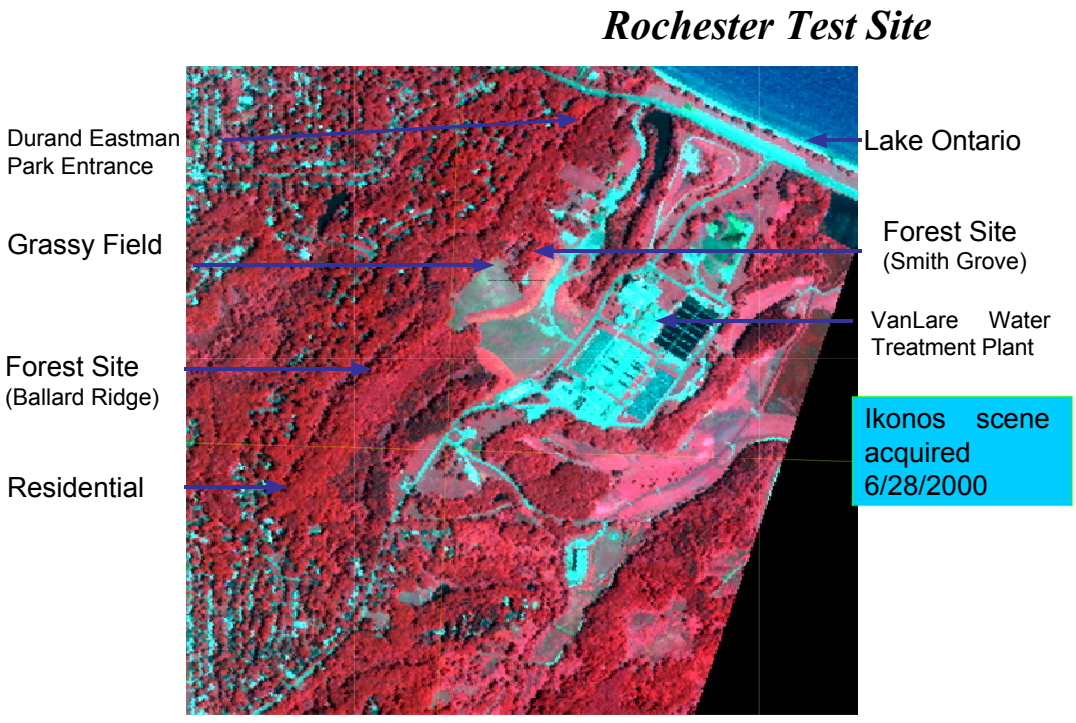

Figure 1. Ikonos Image of Rochester, NY Area

The ETM+ image was on the WRS2 path 16, row 30 scene at 15:40:12 GMT, while the ALI was approximately one minute behind at 15:41:08 GMT. We received the ETM+ L0R data product from the USGS EROS Data Center (EDC) via the EOS Data Gateway. The L0R scene is essentially a raw, but band separated, data product. We applied standard radiometric and geometric corrections to create L1R datasets using our local copy of the EDC Image Assessment System. Full details of the data formats and radiometric and geometric processing are provided in the Landsat 7 Science Data Users Handbook. We received the ALI Level 1 data product from the EO-1 Science Validation Facility at NASA's GSFC. The ALI Level 1 product has been radiometrically, but not geometrically corrected. Our study area was fully imaged by subchip assembly #4, and thus was affected by 3 inoperable detectors in band 5. We interpolated across these inoperable detectors.

We converted the ETM+ and ALI data numbers (DN) to atmospherically corrected reflectance (ACR) by a multi-step process. We first converted each data product from scaled radiance to at sensor radiance (units $W/m^2/sr/\mu m$) by using calibration factors and dividing the ALI image values by 30 and the ETM+ values by 100. We monitored the atmospheric properties using a Cimel sun photometer that was part of the Aerosol Robotic Network (AERONET). It measured the aerosol optical thickness (AOT) at 670nm and 500nm and water vapor column density approximately every 15 minutes. We interpolated these AOT measurements to 550nm and to the image acquisition times to give an AOT of 0.09. We similarly obtain a water content of 1.85 g/cm^2. For ozone content, we used National Center for Environmental Prediction (NCEP) data, which provides ozone data every 6 hours. We interpolated the nearest two measurements to obtain an ozone content of 0.30 cm-atm.

We ran the 6S atmospheric correction code for each of the 15 ALI and ETM+ bands using these measures of the atmospheric conditions and assuming a continental aerosols model. In this mode 6S generates the coefficients xa, xb, and xc that convert the measured at sensor radiance in each band to atmospherically corrected surface reflectance (ACR) via the following equations:

$$y = xa * radiance - xb$$

$$ACR = y / (1 + xc * y)$$

In Tables 1 & 2 below, we show the center wavelength, bandwidth, and the 6S-derived xa, xb, and xc correction coefficients for each of the ETM+ and ALI bands.

Table 1. Bandpass and Atmospheric Correction Parameters for the VNIR Bands

	ALI 1'	ALI 1	ETM+ 1	ALI 2	ETM+ 2	ALI 3	ETM+3	ETM+ 4	ALI 4	ALI 4'
Center λ	0.442	0.485	0.483	0.567	0.56	0.660	0.662	0.835	0.790	0.866
Bandpass	.43-.45	.45-.51	.45-.51	.53-.60	.52-.60	.63-.69	.63-.69	.77-.90	.78-.80	.84-.89
xa	0.0032	0.0028	0.0028	0.0029	0.0029	0.0032	0.0032	0.0045	0.0039	0.0045
xb	0.1404	0.0932	0.0989	0.0507	0.0528	0.0271	0.0270	0.0119	0.0135	0.0097
xc	0.1868	0.1466	0.1520	0.0950	0.0980	0.0630	0.0627	0.0349	0.0394	0.0314

Table 2. Bandpass and Atmospheric Correction Parameters for the SWIR and Panchromatic Bands

	ALI 5'	ETM+ 5	ALI 5	ETM+ 7	ALI 7	ETM+ pan	ALI pan
Center λ	1.244	1.648	1.640	2.206	2.226	0.705	0.592
Bandpass	1.20-1.29	1.55-175	1.55-1.73	2.07-2.35	2.09-2.36	0.52-0.90	0.50-0.68
Xa	0.0101	0.0199	0.0194	0.0598	0.0612	0.0036	0.0030
Xb	0.0037	0.0017	0.0017	0.0007	0.0007	0.0280	0.0461
Xc	0.0148	0.0080	0.0081	0.0037	0.0037	0.0618	0.0895

Visual Image Comparisons

We extracted a 320 x 320 pixel subimage that includes the Durand Eastman Park, Lake Ontario, Irondequoit Bay, and NE Rochester. In Figure 2 below, we show true color composites of the atmospherically corrected reflectance images using bands 3, 2, and 1 of the ETM+ (left) and ALI (right). We use identical linear color transfer functions that exclude the highest and lowest 2% of the pixel histograms. We present Level 1R data from both instruments to maximize radiometric fidelity, which means that slight geometric displacements are visible in the ETM+ image, and that north is not precisely up.

Qualitatively the ETM+ and ALI images are nearly indistinguishable. We can see more detail in Lake Ontario because of the 12-bit quantization of the ALI data. Interestingly, we can use the ~one minute separation between the images to conclude that the ship near the pier in the ETM+ image is entering Lake Ontario at roughly 24 knots.

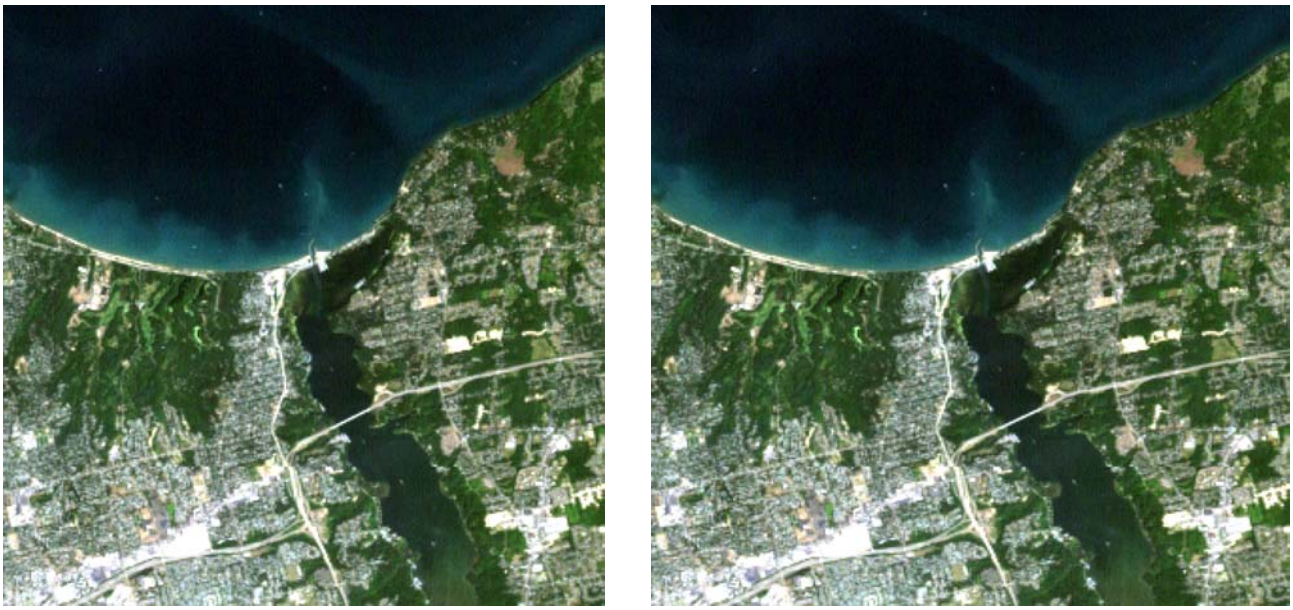

Figure 2. True Color Composites (Bands 3, 2. & 1) – ETM+ (Left) and ALI (Right)

We illustrate the differences in the ALI and ETM+ panchromatic bands in Figure 3 below which shows Irondequoit Bay and the pier into Lake Ontario. The ALI data provide better definition of the marina and pier, and much more detail in the water features of both Lake Ontario and Irondequoit Bay. Three effects

are responsible for the improvement in the ALI panchromatic image: the increase in resolution from 15m to 10m, the increase to 12-bit quantization, and the narrowing of the bandpass. The 12-bit quantization is most responsible for the improved water detail. With a bandpass that cuts off at 0.7μm the ALI image excludes the sharp vegetation rise, which leads to a darkening of vegetation features and improved contrast.

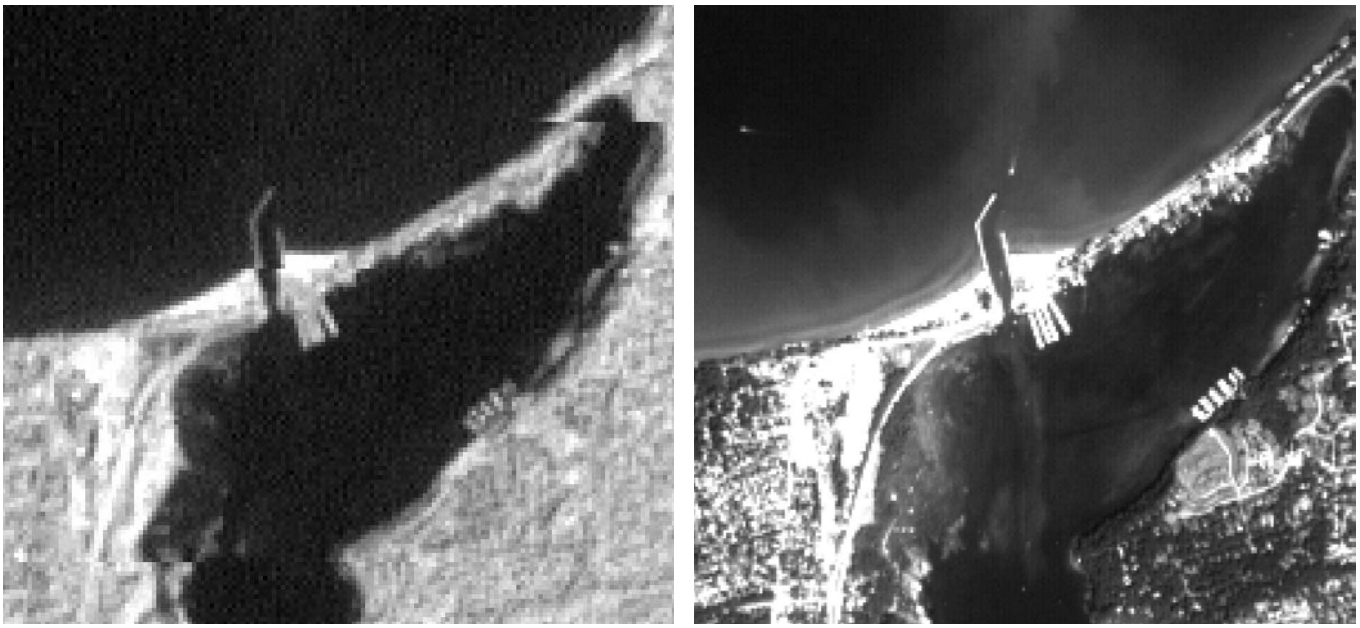

Figure 3. Panchromatic Bands – ETM+ (Left) and ALI (Right)

Spectral and NDVI Comparisons

We extracted 4 pixels each from the ALI and ETM+ images from a reasonably uniform grass region and from the Ballard Ridge forest test site, which we judged by eye to be common between the scenes. We found the overall agreement in spectral response is very good. The largest percent difference is 6% for band 1, but this is only an absolute reflectance difference of 0.005. All other bands agree to within 5%, and the agreement in the SWIR (bands 5 and 7) is ~2%. We find that the formal uncertainty in these reflectance spectra due to the 6S atmospheric correction process is at most ~1.5%, as evaluated by the sensitivity study described above. The uncertainty is largest in the shortest wavelength bands and decreases to less than 0.5% in bands 5 and 7. We note that the new ALI band 5' measures near the peak of the reflectance spectrum, which is unsampled in the ETM+ data.

We calculated the NDVI by calculating the normalized difference between the near infrared and red reflectance values. Figure 4 below are NDVI images calculated from the ETM+ data (left) using bands 4 and 3, and from the ALI (right) using the average of bands 4 and 4' along with band 3. We see the two NDVI images are very similar over land, e.g. both histograms peak at an NDVI value of 0.88 because of the vegetation response. However, we see significant differences between the two sensors in water regions where the signal is very low. We clearly see black and white speckle in the ETM+ data for Lake Ontario, while the ALI is able to distinguish real details in the suspended sediments. The NDVI images show the superior signal to noise of the ALI instrument because of its 12-bit quantization.

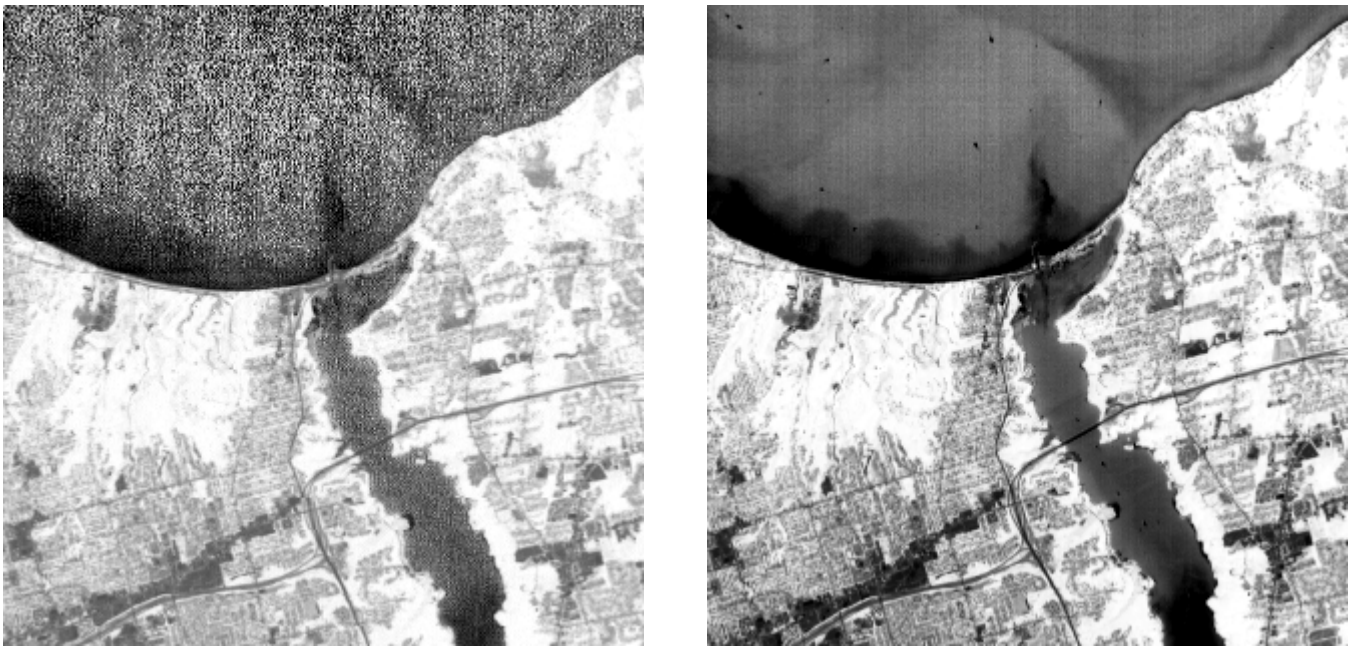

Figure 4. NDVI Inages – ETM+ Bands 3 & 4 (Left) and ALI Bands 3 & 4/4' (Right)

Our results show good qualitative agreement between the multispectral sensors and a significantly improved ALI panchromatic band. We find ≤ 6% differences in the visible/NIR and ~2% differences in the SWIR between the ALI and ETM+ spectral response. Principal component analyses (not reported here) for each sensor indicate that the ALI is able to reproduce the information content in the ETM+ but with superior signal to noise performance because of its increased 12-bit quantization.

Bidirectional Reflectance Distribution Function (BDRF) and Thermal Infrared Modeling of Scenes Imaged with EO-1 and MTI

A second objective of our work is to model the BDRF and thermal infrared characteristics of terrain features at hyperspectral and thermal infrared wavelengths and compare our results to atmospherically corrected EO-1 Hyperion and MTI observations. We selected the Ballard Ridge forest site for intensive measurement and sampling of tree geometry and canopy structure for use in our simulation models. An atmospherically corrected false color composite of the Hyperion image acquired over the area on August 25, 2001 and of a thermal infrared composite of bands L (8.0-8.40 μm), M (8.4-8.85 μm), and N (10.20-10.70 μm) from the MTI acquired on September 9, 2001 are shown below in Figures 5 & 6 respectively.

We used the 6S atmospheric correction code, driven by the Aeronet Sensor, as described above, to correct the Hyperion data. We also have applied the FLAASH atmospheric correction code based on MODTRAN and driven by atmospheric parameters extracted from the Hyperion observations. This is not discussed here, but we are actively researching the application of several atmospheric correction techniques.

Figure 5.
Hyperion Image Acquired August 25, 2001

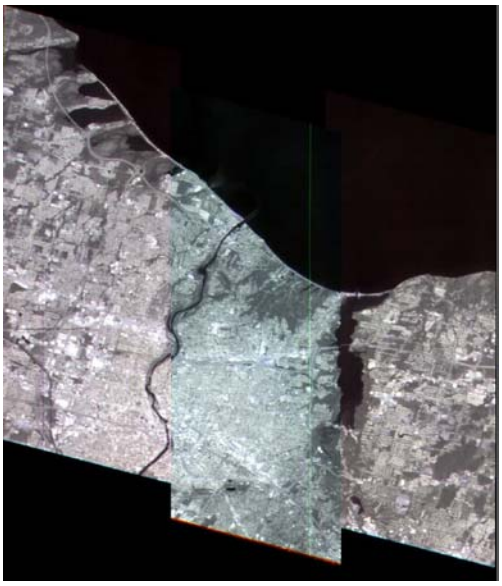

Figure 6.
MTI Image Acquired September 9, 2001

During August and September of 2001, we conducted a detailed survey of the trunk locations, trunk diameter at 1.5 m, crown diameter, canopy dominance (lower, middle, and upper), and species type of approximately 100 trees located within a 30-meter radius.

Plant area index and leaf angle distributions were estimated using indirect optical techniques including the LAI-2000 LAI-meter and hemispherical digital photography. The digital hemispherical photographs were analyzed using Gap Light Analyzer software. The average leaf area index (LAI) from both methods was 4.5.

Detailed geometric measurements of trunks, branches, leaves, leaf clusters, branching angles, and branch length were collected from several trees representing different levels of canopy dominance. These mensuration parameters were then used to generate several geometric tree models. Using the site characterization data, a scene was constructed over a large area that approximated the physical properties of the study site canopy. The resulting tree models were randomly placed at multiple (47,600 trees) locations over a 2 by 2 km area to model the same spacing and density as measured at the study site.

To simulate the reflective wavelengths, we employ simple ray tracing of the reflective and transmissive flux between all scene elements to the sensor. The direct and diffuse flux incident on the canopy are specified and the resulting flux scattered back to the sensor. For the thermal wavelengths, first the temperature distribution of foliage elements are estimated from energy balance models driven by measured meteorological parameters, and then ray-tracing is applied to project thermal exitance from the scene elements into the sensor field of view.

Results

Figure 7, on the left below, is a simulation of the scene at visible wavelengths using a perspective projection out to 45 deg and a viewer position 30 m above the canopy. The solar reflective hot spot can be seen near the upper center of the image. The height of the modeled trees has been varied to match the measured variation in measured tree height at the study site.

Figure 8, on the right, shows the simulation of the scene in the shortwave infrared, 1.55 – 1.73 micrometers. This image is a hemispherical projection out to 90 deg with the viewer 30 m above the canopy. For this short-wave infrared image we also used measured spectral data for the ground, leaves, trunks, and grass in the simulation. In this image the reflective hot spot can be seen approximately 4 deg west of north; this matches the modeled solar azimuth for August 24 at the study site.

Figure 7. Simulation at Visible Wavelengths

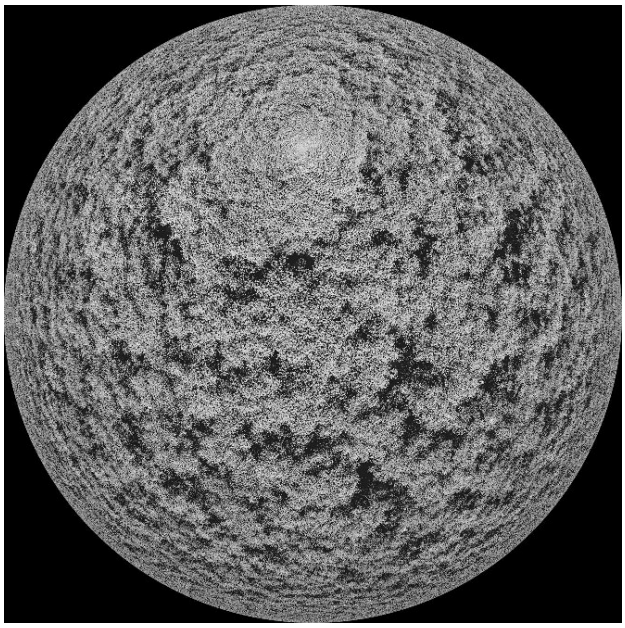

Figure 8. Simulation at Shortwave Infrared Wavelengths

Finally, the Figure 9 below shows the simulation of the canopy in the MTI band M (8.40 – 8.85 micrometers) We have increased the contrast to illustrate the differences in radiance from the sunlit to shaded tree crowns. Gaps in the canopy are much cooler than the surrounding foliage and appear dark. In this high-density canopy (LAI 4.5) the tree trunks, branches, and stem signatures are not easily seen**.**

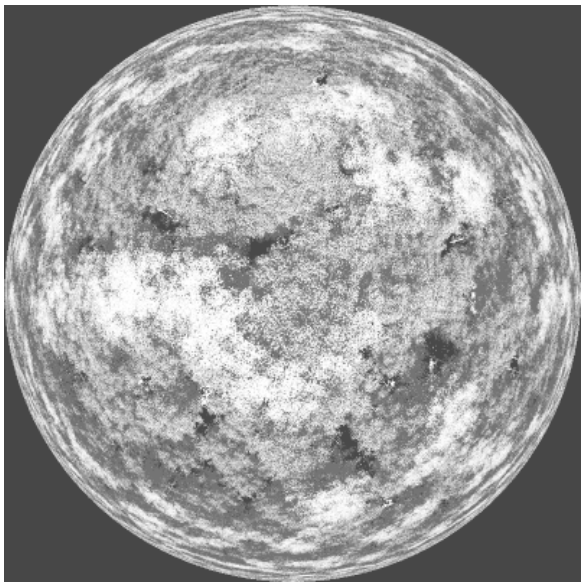

Figure 9. Simulation of Canopy in MTI Band M (8.40 – 8.85 μm)

Acknowledgements

Mr. J. R. Ballard, Jr., U. S. Army Research and Development Laboratory, Dr. J. A. Pedelty and Dr. J. T. Morisette, NASA Goddard Space Flight Center, Dr. S. M. Goltz, University of Maine, and Dr. Lee K. Balick, Los Alamos National Laboratory made major contributions to the work reported here.

Mr. Brent Holben, NASA Goddard Space Flight Center, provided the AERNONET sun photometer at Rochester and Howland. Mr. Don Ho, SSAI, installed the photometer at Rochester during the field campaign and assisted with field measurements. Field spectra at Rochester and other technical assistance were obtained by Ms. Nina Raqueño and Dr. John Schott, Rochester Institute of Technology.

References

J. A. Pedelty, J. T. Morisette, and J. A. Smith, *"*Comparison of Landsat-7 ETM+ and EO-1 ALI*," Opt. Eng*. 2003 (In Review)

J. R. Ballard, Jr. and J. A. Smith, "Hyperspectral canopy reflectance modeling and EO-1 Hyperion," SPIE Conference, Orlando, FL, 1-5 April 2002.

J. R. Ballard, Jr. and J. A. Smith, "A multi-wavelength thermal infrared and reflectance scene simulation model," Proc. IEEE Intl Geosci. and Rem. Sens. Symposium 2002, Toronto, Canada, 24-28 June 2002.

Chein-I Chang, Shao-Shan Chiang, James A. Smith, and Irving W. Ginsberg "Linear spectral random mixture analysis for hyperspectral imagery," *IEEE Trans. Geosci. and Rem. Sens*. 40(2):375-392, 2002.

James A. Smith and Jerrell R. Ballard, Jr., "Thermal infrared hot spot and dependence on canopy geometry," *Opt. Eng*. 40, pp. 1435-1437, 2001.